J Therm Anal Calorim (2009) 97:223–229
DOI 10.1007/s10973-009-0260-8

Role of the dispersion route on the phase transformation of a nano-crystalline transition alumina

Paola Palmero · Barbara Bonelli · Fernando Lomello · Edoardo Garrone · Laura Montanaro

ICTAC2008 Conference

Abstract De-agglomeration of a nanocrystalline transition alumina powder was performed in distilled water at its natural pH under magnetic stirring for 170 h or by ball milling for 3 h. Gibbsite appeared near transition aluminas in the magnetic stirred sample. In addition, a relevant lowering of the α-Al_2O_3 crystallization temperature was observed in the dispersed materials with respect to the as-received powder. However, the activation energy of the above transformation, determined by the Kissinger method, was in any case about 480–500 kJ/mol and unaffected by the dispersion route. On the contrary, it was reduced of about 10% in α-alumina seeded samples, obtained by flash plunging the powders at 1,290 °C for 10 min.

Keywords Crystallization kinetics · Dispersion · Nanocrystalline transition alumina · Thermal evolution

Introduction

Compared to the respective coarse-grained ones, nanocrystalline powders can exhibit enhanced sinterability, so that highly dense ceramics with tailored, ultra-fine microstructures could be prepared [1, 2]. However, nano-sized ceramic powders are often heavily agglomerated and their dry forming leads to green microstructures which are affected by two types of pores: micronic inter-agglomerates pores, and nanometric inter-crystallites ones, within the agglomerate itself. During sintering, the elimination of inter-agglomerates pores needs high temperatures, thus encouraging grain growth [3]. As a matter of fact, agglomeration-free particles and narrow size distributions are imperative requirements for nanosized powders to be consolidated into highly dense, fine microstructures [2]. Moreover, well-dispersed metastable powders should exhibit a relevant lower transformation temperature to the final, thermodynamically stable phase as compared to the respective agglomerated material [4]. As an example, a de-agglomeration route has been successfully exploited for lowering the transformation temperature of transition alumina, which normally occurs at temperatures higher than 1,200 °C. However, phase transformation is accompanied by a finger or vermicular grain growth of the α-particles [4], so that the production of well-dispersed and nano-sized α-Al_2O_3 powders from calcination of transition ones is almost impossible. A variety of methods have been applied to transition alumina for improving transformation kinetics and lowering α-phase nucleation temperature. Among them, seeding has been extensively reported in literature [5–7]. In fact, according to previous studies, addition of seeds such as α-Al_2O_3, α-Fe_2O_3, TiO_2, provides low-energy sites for heterogeneous nucleation and thus reduces the energy barrier required for nucleation. Finally, in some works, de-agglomeration and seeding effects were coupled in a synergic way, thanks to the fact that during grinding, fine α-alumina grains from the milling media contaminate the starting powder [8, 9].

In the present paper, modifications of a commercial nanocrystalline transition alumina powder were induced by a dispersion step and/or by thermal-mechanical pre-treatments. However, in contrast to previous papers, the main purpose

P. Palmero (✉) · F. Lomello · L. Montanaro
Politecnico di Torino, Department of Materials Science and Chemical Engineering, INSTM—R.U. PoliTO—LINCE Lab, Corso Duca degli Abruzzi, 24, 10129 Torino, Italy
e-mail: paola.palmero@polito.it

B. Bonelli · E. Garrone
Politecnico di Torino, Department of Materials Science and Chemical Engineering, INSTM—R.U. PoliTO, Corso Duca degli Abruzzi, 24, 10129 Torino, Italy

of this work was to clarify the overall effect of the dispersion on many chemical, physical and thermal features of the starting material, such as phase composition and evolution, surface properties, and θ to α-Al_2O_3 transformation kinetics. In addition, for investigating the role of dispersion and seeding in a separate way, five different materials were produced. Precisely, three powders were dispersed up to achieve almost the same agglomerate size distribution, but under different dispersion conditions, i.e., ball-milling by using α-alumina or zirconia spheres, which can induce a certain amount of pollution from the milling media, or under magnetic stirring, for producing a completely un-polluted sample. Finally, in the last two materials, a limited amount of α-alumina phase was yielded into the as-received powder, by flash plunging it at 1,290 °C for 3 or 10 min, respectively.

Materials and methods

A commercial, nano-crystalline transition alumina (Nanotek® by Nanophase Technologies Corporation, Darien, IL, USA), was used as starting material and labelled A from now on. The main physico-chemical features of the as-received powder, given by the supplier (http://www.nanophase.com), are reported in Tables 1 and 2. In Fig. 1, a TEM micrograph of A is shown, confirming the ultra-fine size of the primary particles as well as their spherical morphology.

The phase transition from θ to α-Al_2O_3 was investigated by simultaneous DTA-TG analysis (Netzsch STA 409C), performed up to 1,400 °C in static air, at a heating rate of 10 °C/min. On the contrary, the other lower-temperature phase transformation (i.e., from γ to δ and then to θ) do not give rise to calorimetric signals because of topotactic phenomena.

Table 1 Main physico-chemical features of A (http://www.nanophase.com)

Purity	99.95%
Average particle size	47 nm
SSA (BET)	35 m^2/g
True density	3.49 g/cm^3
Morphology	Spherical
Crystal phases	70%:30%; δ:γ

Table 2 Activation energy (E_a) for θ to α-Al_2O_3 phase transformation and squared linear correlation coefficient of the Kissinger plot

Sample	E_a/kJ mol^{-1}	r^2
A	486	0.9959
A_{MS}	498	0.9946
$A_{BM\alpha}$	480	0.9969
A_{BMz}	496	0.9993
$A_{\alpha 3}$	502	0.9892
$A_{\alpha 10}$	438	0.9990

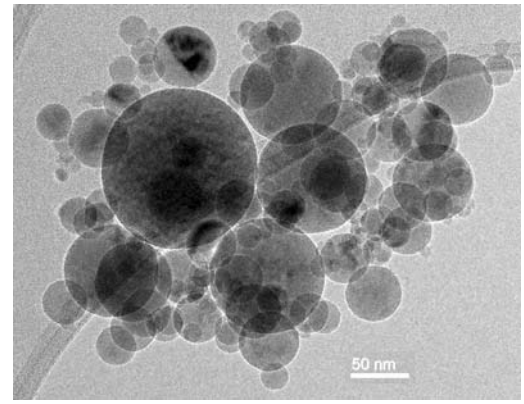

Fig. 1 TEM image of A

The powder composition was evaluated by X-ray diffraction (XRD, Philips PW 1710), in the range 5–70° 2θ, with a step size of 0.05° 2θ and an acquisition time per step of 5 s. The starting agglomerate size distribution in water suspension was evaluated by a laser granulometer (Fritsch Analysette 22 Compact), while TEM (JEOL 3010-UHR) observations allowed to determine the particle size distribution from several image analyses. Powder A was dispersed in distilled water (solid content of 50 wt%), at its natural pH of about 5.5, and maintained under magnetic stirring in a PTFE equipment up to 170 h (samples labelled as A_{MS}) or ball-milled up to 3 h, by testing both α-alumina (Bitossi; diameter = 2 mm, $A_{BM\alpha}$) and zirconia (TSZ TOSOH, diameter = 1.75 mm, A_{BMz}) spheres (powder to spheres mass ratio of 1:10). The dispersion was stopped when a similar particle size distribution was achieved from both routes as stated by laser granulometer analyses performed as a function of the dispersion time. FTIR measurements were performed on A and A_{MS} samples, by pressing the powders into self-supporting wafers. Spectra were collected at a resolution of 2 cm^{-1} in the 4,000–1,000 cm^{-1} range, by using Bruker FTIR Equinox 55 spectrophotometer equipped with a MCT detector. Pre-treatments were carried out using a standard vacuum frame in a IR cell equipped with KBr windows. To remove water and other atmospheric contaminants, wafers were out-gassed for 1 h at increasing temperatures (150, 350 and 500 °C) before any IR investigations. As-received and dispersed powders were calcined at 1,000, 1,150 and 1,200 °C for 30 min with a heating rate of 10 °C/min, and phase evolution was followed by XRD analyses. Powder A was also submitted to a different heating cycle, stated on the ground of its DTA curve, in order to partially crystallize α-alumina phase. For minimizing the crystallite growth, the powders were plunged for 3 or 10 min into a tubular furnace, kept at 1,290 °C, and labelled as $A_{\alpha 3}$ and $A_{\alpha 10}$, respectively.

The activation energy of phase transformation for A, $A_{\alpha 3}$, $A_{\alpha 10}$, A_{MS}, $A_{BM\alpha}$ and A_{BMz} samples was determined by using Kissinger' kinetics model [10], in which DTA signals recorded for 100 mg-powdered samples at various heating rates (namely, 5, 10, 15 and 20 °C/min) were exploited. Kinetics parameters were determined by the Kissinger equation (1):

$$\ln\left[\frac{\left(\frac{dT}{dt}\right)}{T_m^2}\right] = \frac{E_a}{R}\left(\frac{1}{T_m}\right) + B \quad (1)$$

where $B = \ln(AR/E_a)$ is a constant, T is the temperature in K, t is the time (in min), T_m is the DTA peak maximum temperature of the phase transformation, E_a is the activation energy, A is the Arrhenius constant, and R is the gas constant. Plotting $\ln[(dT/dt)/T_m^2]$ vs. $(1/T_m)$, activation energy can be calculated from the curve slope.

Results and discussions

Powder A is a mixture of transition alumina phases, precisely δ-Al_2O_3 (ICDD file no. 04-0877) and γ-Al_2O_3 (ICDD file no. 48-0367), as determined by XRD. θ-Al_2O_3 (ICDD file no. 11-0517) phase started to appear after calcination at 1,150 °C for 30 min, while traces of α-alumina (ICDD file 10-0173) were detected only after treatment at 1,200 °C for 30 min. Finally, the powder calcined at 1,300 °C for 30 min was a pure α-Al_2O_3 phase.

Image analyses from TEM observations (Fig. 1) allowed to define the size distribution of primary particles, as reported in Fig. 2a. A mean size of about 37 nm was determined, with a geometrical standard deviation of 20.5 nm. Figure 2b, indeed, shows the cumulative agglomerate size distribution by volume of A, from which sizes of 2.5, 8.0 and 15.7 μm, corresponding to 10 (d_{10}), 50 (d_{50}) and 90 (d_{90})%, respectively, of the cumulative distribution, were determined. A significant reduction of the above sizes were evaluated for A_{MS}, $A_{BM\alpha}$ and A_{BMz} samples, characterized by quite superimposable distributions, as shown in Fig. 2b. In the inset of the same figure, d_{50} values for A and for the dispersed powders are compared.

A significant effect of the de-agglomeration process in lowering the crystallization temperature of the α-phase was put in evidence by performing DTA analysis on all the powders (Fig. 3a). Powder A shows a broad exothermal signal, whose peak temperature was at about 1,325 °C, imputable to the crystallization of the α-phase from θ-Al_2O_3, as reported in literature [11] and also confirmed by XRD analyses performed on the powder calcined around the above temperature value. The thermal evolution is associated to a limited mass loss of about 1.3%, as recorded by the TG curve.

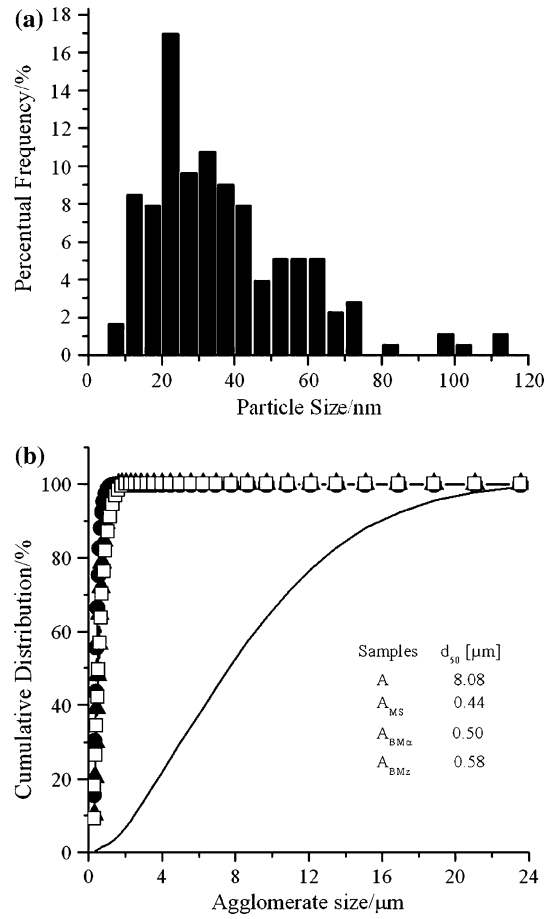

Fig. 2 **a** Particle size distribution of A by TEM observation; **b** cumulative agglomerate size distribution by volume of A (*solid line, no symbols*), A_{MS} (*circles*), $A_{BM\alpha}$ (*triangles*) and A_{BMz} (*squares*). *Inset* d_{50} values of the overall distributions

Dispersion induced a lowering of the transformation temperature, in a good agreement with a previous study [4], since sharp exothermal signals were detected at 1,203, 1,180 and 1,210 °C for A_{MS}, $A_{BM\alpha}$ and A_{BMz} samples, respectively. It should be observed that, in spite of the same degree of de-agglomeration was induced in the three dispersed powders, a relevantly lower transformation temperature was detected in $A_{BM\alpha}$, as it will be discussed in the following.

From Fig. 3a, a further difference among A and the dispersed samples should be observed in the low-temperature regime. In fact, DTA curves of dispersed powders present a new broad endothermic signal in the range 280–290 °C, accompanied by an abrupt mass loss, as show in Fig. 3b which collects the TG-DTG curves of A_{MS} in the 100–600 °C range.

The different thermal behavior between A and the dispersed powders was associated to different starting phase compositions, as evidenced by the XRD patterns reported in Fig. 4. A and the ball-milled powders were purely made of

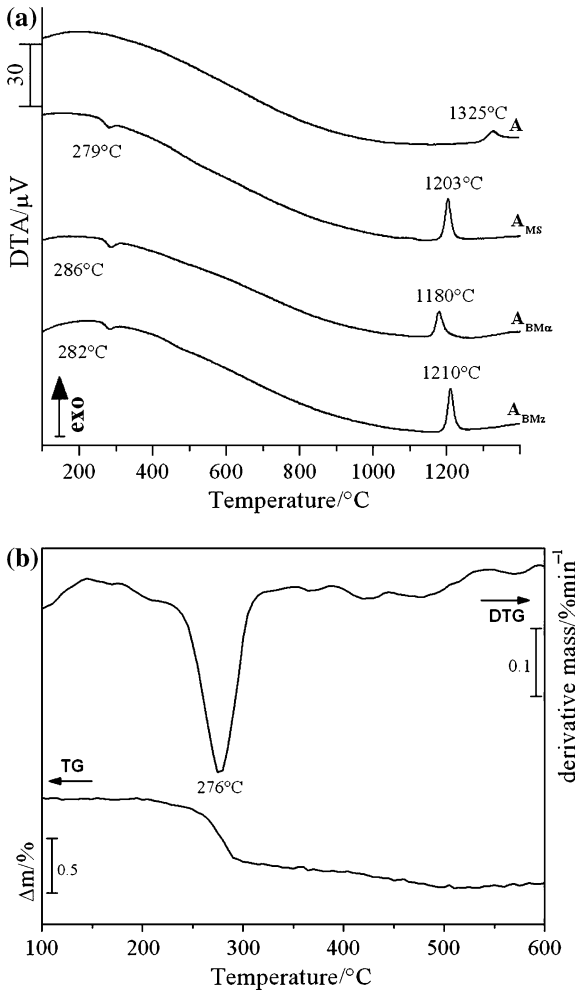

Fig. 3 **a** DTA curves of A and of the dispersed samples; **b** TG–DTG curves of A_{MS} in the 100−600 °C range

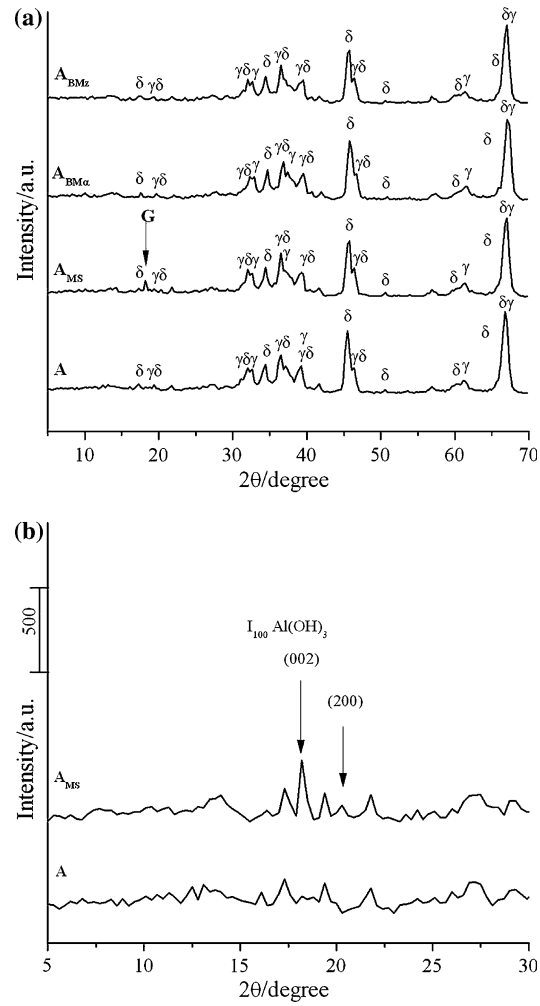

Fig. 4 **a** XRD pattern of A and of the dispersed samples (G = gibbsite); **b** XRD pattern of A and A_{MS} in the 5–30° 2θ range (*arrows* indicate gibbsite peaks)

transition alumina phases (γ and δ-Al_2O_3); no XRD reflections imputable to α-Al_2O_3 or zirconia phases were determined in $A_{BM\alpha}$ and A_{BMz}, respectively, showing that pollution from the milling media, if present, was lower than the instrumental detection limit. On the contrary, in A_{MS} near transition aluminas the main peaks of gibbsite ($Al(OH)_3$, ICDD 76-1782) were determined, whose formation was imputed to the prolonged dispersion process in aqueous suspension, as already reported in literature [12]. The 5–30° 2θ range, in which the main XRD reflections of gibbsite appear, is better evidenced in Fig. 4b, which compares A and A_{MS} spectra. To confirm the above statement, XRD analyses were also performed on samples dispersed under magnetic stirring for 24, 36, 48 and 72 h; the major peaks of aluminum hydroxide appear after 24 h of magnetic stirring but their intensities remain almost constant up to 172 h of dispersion. Moreover, after calcining A_{MS} at 350 °C for 30 min, gibbsite reflections disappeared, confirming that the endothermic DTA signal of the stirred material could be reasonably imputed to its thermal decomposition. The amount of gibbsite formed upon hydration of transition alumina could be estimated from the mass of water evolved at about 280 °C, given by TG data, according to the reaction:

$$Al(OH)_3 \rightarrow AlOOH + H_2O.$$

As an example, A_{MS} underwent to a mass loss of about 0.64% (see Fig. 3b), leading to a gibbsite content in the starting material of about 3%.

In Fig. 5, the FTIR spectra of A (a) and A_{MS} (b) samples recorded at room temperature (RT) and after out-gassing at 150, 350 and 500 °C, respectively, are collected. Molecular water (band at 1,628 cm^{-1}) is removed from sample A_{MS} at RT, whereas a higher temperature treatment (150 °C) is necessary to remove water from sample A. Carbonates

(bands in the 1,700–1,250 cm^{-1} range) also showed a different behaviour. At 500 °C they are still stable in the dispersed sample, whereas completely removed in the as-received powder. As a whole, the main differences between the two samples, as derived from a comparison between the spectra recorded after the same thermal treatment, are: (i) before magnetic stirring, stronger adsorption sites are present, to which water molecules may coordinate (most probably Al^{3+} or hydroxyls); (ii) after magnetic stirring, stronger basic sites (oxygens) to which CO_2 coordinates are present (carbonates stable up to 500 °C). FTIR revealed that surface was modified in A_{MS}, becoming more hydrophobic as well as more basic compared with A, probably due to the formation of the outer gibbsite layer. In the OH-stretch range, bands are seen of hydroxyls species usually observed at the surface of transition aluminas, as reported in literature [13].

The dispersion route was also effective in modifying the high-temperature crystallization path of the materials, as evidenced by XRD analyses performed on A and on the dispersed samples, calcined at 1,000 and 1,150 °C for 30 min. After calcination at 1,000 °C for 30 min (Fig. 6a), A is a mixture of γ, δ and θ-phases, while in the dispersed samples near transition aluminas also traces of α-Al_2O_3 were detected, with a higher peak intensity in $A_{BM\alpha}$ as regards to the other dispersed samples. This effect should be imputed to a seeding effect from the milling media which, even if undetectable by XRD performed on the as-dispersed material, should promote α-alumina crystallization when the material is treated at high temperature.

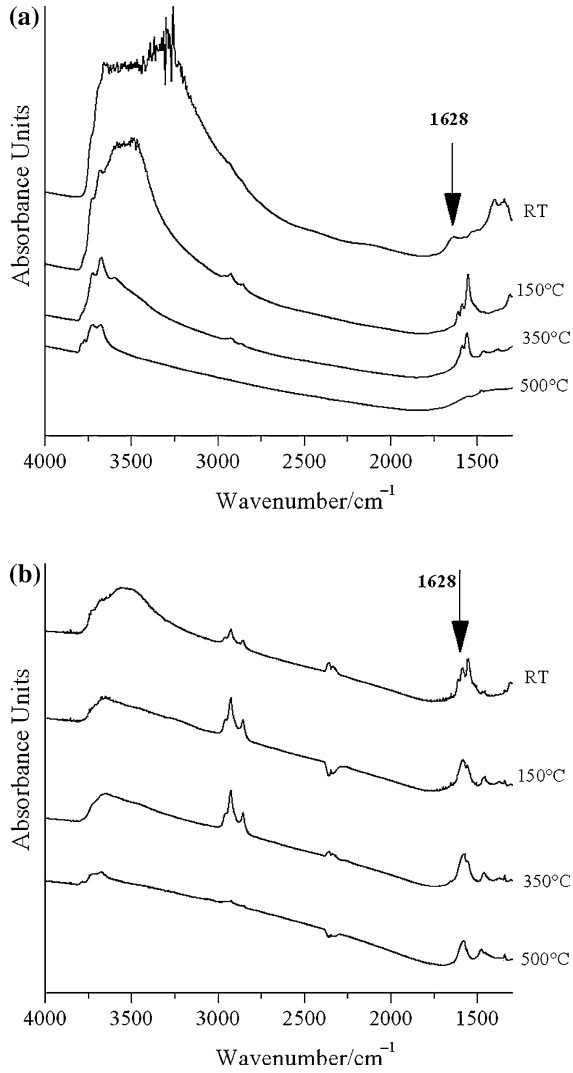

Fig. 5 FTIR spectra of **a** A and **b** A_{MS} recorded at RT and after outgassing at 150, 350 and 500 °C

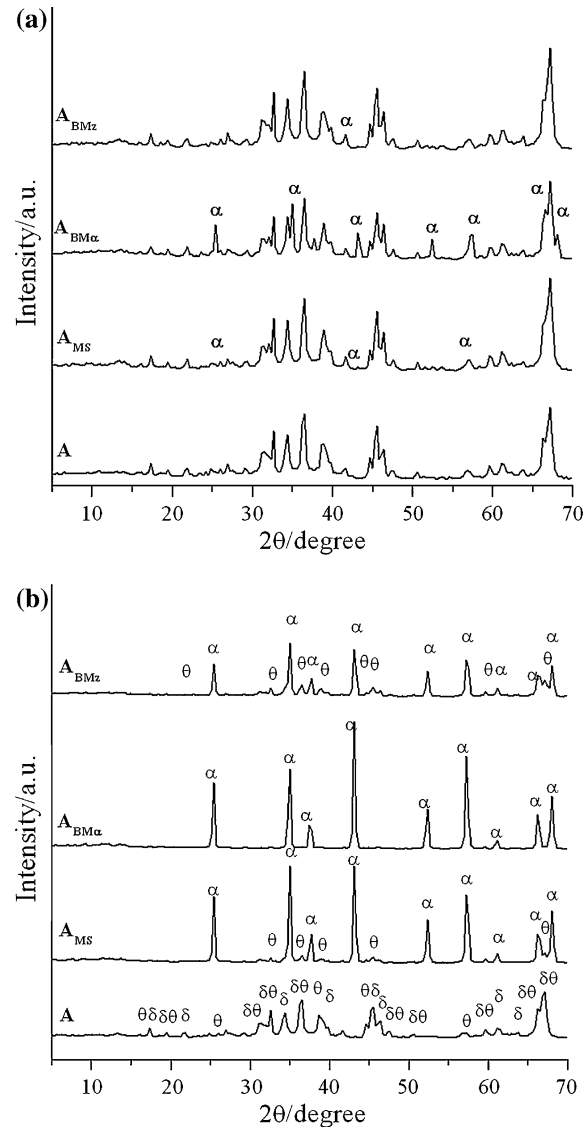

Fig. 6 XRD pattern of A, A_{MS}, $A_{MB\alpha}$ and A_{BMz} calcined at **a** 1,000 °C and **b** 1,150 °C for 30 min. For a sake of clarity, only the α-phase was labelled in **a**

After calcination at 1,150 °C (Fig. 6b), A was still made of pure transition phases (namely δ and θ-phases); in A_{MS}, α-Al_2O_3 was the prevalent phase near θ-Al_2O_3; a pure, well-crystallized α-Al_2O_3 was detected in $A_{BM\alpha}$ and finally, A_{BMz} was a mixture of transition and α-Al_2O_3 phases. The relevant difference in phase composition between $A_{BM\alpha}$ and A_{BMz}, having the same starting particle size distribution, should be, once again, imputed to the different pollution effect from the milling media which can, respectively, promote or delay their α-alumina transformation. This hypothesis will be better deepened in the following.

The Kissinger plots of phase transformation in A and in the dispersed samples, by fitting to Eq. 1, are shown in Fig. 7 and the related activation energies are collected in Table 2. By comparing curves I, IV, V and VI, the significant role of the dispersion process in lowering the transformation temperature can be observed. By keeping the un-polluted stirred sample, A_{MS}, as a reference, it could be observed that the lowering of the transformation temperature in $A_{BM\alpha}$ was more relevant if compared to the weak delaying effect presented by A_{BMz}.

For investigating the role of seeding on the above transformation, kinetics plots were also determined for $A_{\alpha 3}$ and $A_{\alpha 10}$ samples, in which variable amounts of α-alumina phase were produced by flash heating. Figure 8 compares the XRD patterns of $A_{\alpha 3}$ and $A_{\alpha 10}$ in the 38–50° 2θ range; in $A_{\alpha 3}$ the alpha phase was almost undetectable, as in the case of $A_{BM\alpha}$, while an appreciable XRD peak was indeed observed in $A_{\alpha 10}$.

The comparison among the Kissinger plots of A (I) with those of $A_{BM\alpha}$ (VI), $A_{\alpha 3}$ (II) and $A_{\alpha 10}$ (III), shows that also seeding lowers the transformation temperature, and in a more effective way by increasing the α-seeds amount. So,

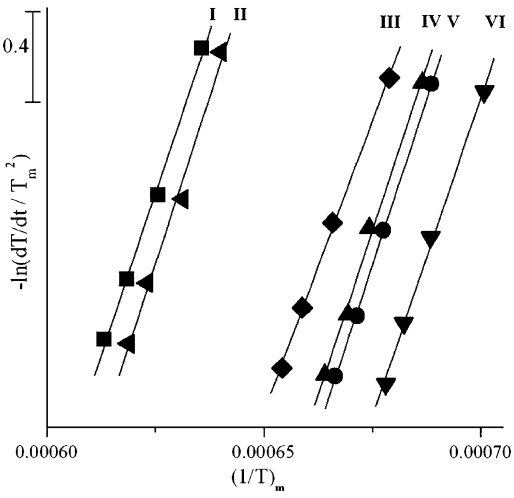

Fig. 7 Kissinger plot of θ to α-Al_2O_3 phase transformation for A (I), $A_{\alpha 3}$ (II), $A_{\alpha 10}$ (III), A_{BMz} (IV), A_{MS} (V) and $A_{BM\alpha}$ (VI)

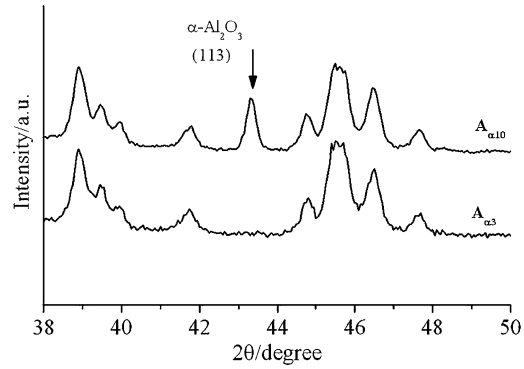

Fig. 8 XRD patterns of $A_{\alpha 3}$ and $A_{\alpha 10}$ in the 38–50° 2θ range

the more pronounced anticipation occurring in $A_{BM\alpha}$ should be reasonably imputed to a positive effect induced by coupling dispersion and seeding with α-phase. On the ground of this hypothesis, also the "delaying" effect of A_{BMz} should be imputed to the pollution effect induced by zirconia milling media, which being a second immiscible phase acts negatively on the transformation temperature, as expected on the ground of literature [14].

Concerning activation energy, also in this case the role of dispersion and seeding should be separately discussed.

The activation energy of A was 486 kJ/mol, in a good agreement with literature data [6], but it was almost unaffected by the dispersion routes. This results is only in partial agreement with literature data, in which a lower θ to α-Al_2O_3 transformation temperature due to an effective dispersion process was also accompanied by a lowering in activation energy [4, 6]. On the contrary, seeding is able to lower the above energy, as shown by $A_{\alpha 10}$, for which a decrease of about 10%, as compared to A, was determined. However, a similar decrease was not presented by $A_{\alpha 3}$ and $A_{BM\alpha}$, thus suggesting that detectable amounts of α-seeds are required to affect the activation energy of the transformation.

As a future activity, optimized processed powders should be produced by coupling the flash heating step to an effective dispersion process, thus to induce a lowering of both transformation temperature and related activation energy. Thus, ultra-fine, agglomerate-free and reactive powders should be employed for sintering highly dense ceramic bodies, with fine and homogeneous microstructures.

Conclusions

Dispersion of a commercial, transition nano-crystalline alumina was successfully performed in distilled water, under magnetic stirring or by ball-milling, carried out by using both α-alumina or zirconia spheres. The dispersion process was effective in modifying the crystallization path, both at low and high temperatures regimes. Gibbsite phase was

determined near transition aluminas in the stirred samples. Moreover, the prolonged dispersion process induced a surface modification in this material, becoming more hydrophobic as well as more basic, as compared with the as-received sample. In the high-temperature regimes, a significant lowering of the α-Al_2O_3 crystallization temperature was determined in all the de-agglomerated materials. In contrast, the activation energy associated to the above phase transformation was unaffected by the dispersion route; however, this value was successfully decreased in a sample in which an appreciable α-phase seeding was induced by a flash heating cycle.

References

1. Mayo MJ. Processing of nanocrystalline ceramics from ultrafine particles. Int Mater Rev. 1996;41:85–115.
2. Ma J, Lim LC. Effect of particle size distribution on sintering of agglomerate-free submicron alumina powder compacts. J Eur Ceram Soc. 2002;22:2197–208.
3. Bowen P, Carry C. From powders to sintered pieces: forming, transformations and sintering of nanostructured ceramic oxides. Powder Technol. 2002;128:248–55.
4. Yang R-J, Yen F-S, Lin S-M, Chen C-C. Microstructure-controlled effects on temperature reduction of α-Al_2O_3 crystallite formation. J Cryst Growth. 2007;299:429–35.
5. Yen FS, Wang MY, Chang JL. Temperature reduction of θ- to α-phase transformation induced by high-pressure pretreatments of nano-sized alumina powders derived from boehmite. J Cryst Growth. 2002;236:197–209.
6. Nordahl CS, Messing GL. Thermal analysis of phase transformation kinetics in α-Al_2O_3 seeded boehmite and γ-Al_2O_3. Thermochim Acta. 1998;318:187–99.
7. Yen FS, Lo HS, Wen HL, Yang RJ. Temperature reduction of θ- to α-phase transformation induced by high-pressure pretreatments of nano-sized alumina powders derived from boehmite. J Cryst Growth. 2003;249:283–93.
8. Xie Z-P, Lu J-W, Gao L-C, Li W-C, Xu L-h, Wang X-D. Influence of different seeds on transformation of aluminum hydroxides and morphology of alumina grains by hot-pressing. Mat Des. 2003;24:209–14.
9. Kano J, Saeki S, Tanjo M, Saito F. Reduction in α-transformation temperature of gibbsiteand boehmite by powder mixing with seed. Reduction in α-transformation temperature of gibbsiteand boehmite by powder mixing with seed. J Chem Eng Jpn. 2001;34:595–9.
10. Kissinger HE. Reaction kinetics in differential thermal analysis. Anal Chem. 1957;29:1702–6.
11. Kao H-C, Wei W-C. Kinetics and microstructural evolution of heterogeneous transformation of θ-alumina to γ-alumina. J Am Ceram Soc. 2000;83:362–8.
12. Carrier X, Marceau E, Lambert J-F, Che M. Transformations of γ-alumina in aqueous suspensions. 1. Alumina chemical weathering studied as a function of pH. J Colloid Interface Sci. 2007;306:429–37.
13. Morterra C, Magnacca G. A case study: surface chemistry and surface structure of catalytic aluminas, as studied by vibrational spectroscopy of adsorbed species. Catal Today. 1996;27:497–532.
14. Lange FF, Hirlinger MM. Hindrance of grain growth in Al_2O_3 by ZrO_2 inclusions. J Am Ceram Soc. 1984;67:164–8.